Structure in numerical simulation of cellular detonations with detailed reaction model

X Y Hu [a] B C Khoo [a] D L Zhang [b] Z L Jiang [b]

[a]*Singapore-MIT Alliance, National University of Singapore, 4 Engineering Drive 3, 117576, Singapore*

[b]*Laboratory of High Temperature Gas Dynamics, Institute of Mechanics, Beijing, 100080, China*

Abstract

In this paper, the structure in two dimensional numerical simulations of cellular detonation waves with detailed chemical reaction model is investigated. By high order schemes and high resolution grid, well resolved, regular cellular structure develops about $1ms$ after introducing perturbations in reaction zone. Good convergence is shown when results are examined with different resolutions. Then, the evaluation process of the structure is studied with high resolution results. The results show that the structure is a double Mach like strong type, but with stronger configuration around the the second triple point. In the triple point collision, three regular reflecting processes are observed taking place firstly, and then followed by a quickly change to the double Mach like configuration. The comparisons with experiments and previous calculation shows the calculated strong structure here is weaker than that of a marginal detonation. However, the results also indicates that even for ordinary detonation there is a strong cellular structure.

Key words:

1 Introduction

It is well known that gaseous detonation wave has cellular structure. Experiments show that smoked foils on channel wall can record the tracks of cellular structure, and the regions enclosed by these tracks are called detonation cells. For regular cellular patterns, which are rectangular and planar modes, these can be idealized to two dimensional approximately. The cellular structure is usually complex and involves triple wave configurations, one of which includes an incident shock wave (I), a Mach stem (M) and a transverse wave (T). Two types of cellular structures are observed in experiments. In a weak structure,

Table 1
Comparisons of
marginal detonation and ordinary detonation

Parameters	Marginal	Ordinary
mean detonation velocity $(\bar{D}/D_{CJ})$	$0.8 \sim 0.9$	~ 1
variation through the cell $(\bar{D}/D_{CJ})$	$1.4 \sim 0.7$	$1.2 \sim 0.85$
Transverse wave strength (S^{a})	≥ 1.5	0.5
Cell width length ratio(d/l)	~ 0.7	$0.5 \sim 0.6$
Transverse wave track angle $(^{o})$	> 33	$30 \sim 33$
Transverse wave track lines	2	1

[a] Transverse wave strength is defined as $S = p/p_o - 1$, in which p and p_o are pressure of the front two sides.

the transverse wave is a single shock wave, while the transverse wave of strong structure can lead to secondary ignition. Detonations themselves are classified into ordinary detonations and marginal detonations. An ordinary detonation is characterized by average detonation velocity close to D_{CJ}, while a marginal one only has about $0.85D_{CJ}$. Detailed comparisons between marginal detonation and ordinary detonation are shown in Tab. 1. After extensive experimental work of VMT (Voitsekhovskii, Mitrofanov and Topchian) (1963) and Strelow and Crooker (1974), it is widely accepted that, in a propagating marginal detonation, the cellular structure is strong type. However, whether ordinary detonation has strong structure or not is not very clear (Fickett and Davis, 1979).

From late 1970's, numerical simulation has been employed to study the cellular structure. In the early works, simple one or two-steps chemical reaction model were used, and the calculated results showed typical triple wave configurations (Taki et al, 1978). Fine spatial resolution numerical simulations with simple reaction models have also been used to study the detailed cellular structure (Quirk, 1993; Gamezo et al, 1999). As chemical reactions are coupled with the self-sustained detonation, more complex chemical reaction model is essential for obtaining greater detailed structure. Recently, multi-step, detailed reaction model have been used with some success and new results computed. With this model Lefebvre and Oran (1995) calculated the triple wave configuration behavior which indicated that the configuration evaluating form single Mach configuration to double, then more complex Mach configuration. Recently, very high spatial resolution numerical simulation with simple reaction models have been used to study detailed cellular structure (Sharpe, 2001). Sharpe argued that the structure just after triple wave collisions is already strong

type comprising double Mach configurations, and then keeps this type for the whole evaluation process.

In this paper, the behavior of the cellular structure is investigated in numerical simulations of two dimensional detonation waves with a detailed reaction model. The regular cellular structure formation process is firstly presented, and resolution studies are performed to examine the convergence property between high resolution results and lower resolution ones. Then the evaluation process of the structure was investigated in detail with very high resolution results. The numerical simulation was also compared with experimental data and previous calculations.

2 Governing equations and chemical reaction model

The governing equations for two dimensional gaseous detonation with N species, multi-step chemical reaction model are

$$\frac{\partial \mathbf{U}}{\partial t} + \frac{\partial \mathbf{F}}{\partial x} + \frac{\partial \mathbf{G}}{\partial y} = \mathbf{S}, \tag{1}$$

where

$$\mathbf{U} = \begin{pmatrix} \rho \\ \rho u \\ \rho v \\ E \\ \rho_1 \\ \vdots \\ \rho_{N-1} \end{pmatrix}, \mathbf{F} = \begin{pmatrix} \rho u \\ \rho u^2 + p \\ \rho u v \\ (E+p)u \\ \rho_1 u \\ \vdots \\ \rho_{N-1} u \end{pmatrix}, \mathbf{G} = \begin{pmatrix} \rho v \\ \rho u v \\ \rho v^2 + p \\ (E+p)v \\ \rho_1 v \\ \vdots \\ \rho_{N-1} v \end{pmatrix}, \mathbf{S} = \begin{pmatrix} 0 \\ 0 \\ 0 \\ 0 \\ \dot{\omega}_1 \\ \vdots \\ \dot{\omega}_{N-1} \end{pmatrix}. \tag{2}$$

This set of equations describes the conservation of density ρ, momentum $\rho \mathbf{v} \equiv (\rho u, \rho v)$, total energy density E, and density of species $\{\rho_i\}$, where $i = 1, N$. To close this set of equation, the total energy density is defined as

$$E = \rho h - p + \frac{\rho(u^2 + v^2)}{2}, \tag{3}$$

where entropy h and pressure p are calculated by thermochemical relation $h = h(\rho_i, T)$ (Stull, 1971), and equation of states $p = p(\rho_i, T)$ for a perfect gas, respectively.

3

For chemical reaction model with K elementary reactions, $k = 1, K$, the chemistry can be described by

$$\sum_{i=1}^{N} \nu'_{ik} \chi_i \rightleftharpoons \sum_{i=1}^{N} \nu''_{ik} \chi_i, k = 1, K, \tag{4}$$

where χ_i is the chemical symbol for species i, and ν'_{ik} and ν''_{ik} are molecularities of species i in kth reaction for reactants and products, respectively. The production rate of each species is given by

$$\dot{\omega}_i = W_i \sum_{k=1}^{K} (\nu''_{ik} - \nu'_{ik}) RP_k, \tag{5}$$

where W_i is molecular weight, and the rate of progress variable of kth elementary reaction, RP_k is defined as

$$RP_k = \left(\sum_{i=1}^{N} \alpha_i C_{\chi i} \right) \left(K_{f,k} \prod_{i=1}^{N} (C_{\chi i})^{\nu'_{ik}} - K_{b,k} \prod_{i=1}^{N} (C_{\chi i})^{\nu''_{ik}} \right). \tag{6}$$

Here α_i is the third body coefficient, $C_{\chi i} = \rho_i / W_i$ is mole concentration of species i, $K_{f,k}$ and $K_{b,k}$ are the forward and backward reaction rate constants, which are controlled by Arrhenius law and chemical equilibrium conditions. It may be noted that for simple chemical reaction model, there is only one or two equation in Eq.(2) with reaction source term, and Eqs.(4)-(6) are replaced by one or two Arrhenius law equations with globe chemistry models (Taki et al, 1978; Gamezo et al, 1999).

In this paper, a 9 species, 19 elementary reactions model is used for hydrogen-oxygen combustion (Wilson and MacCormack, 1990). The reacting species are H_2, O_2, H, O, OH, H_2O_2, HO_2, H_2O, and 70% argon dilute is added to the gas mixture. This gas mixture is selected for numerical simulation primarily because extensive studies on such mixture at low pressure showing regular detonation structure and detonation cells are produced and useful for our comparisons (Fickett and Davis, 1979).

3   Numerical Method

3.1   Numerical schemes and parallelization

This set of coupled partial differential equations is solved by time-step splitting scheme which couples the Euler equations to the chemical reactions (Oran

and Boris, 1987). The contribution from the fluid dynamic terms is firstly calculated to get an intermediate value $\tilde{U}$. This is followed by accounting for the source terms contribution to get U in the next step. This approach allows separate solution of fluid dynamic terms and source terms with different time steps. The implication is that fluid dynamic terms can be integrated by Δt_{fluid} consistent with their CFL condition, and the source terms integrated by a stiff solver valid for chemical kinetic ODE equations by Δt_{source} with required accuracy.

In this paper, the finite difference scheme is based on 3rd order ENO-LLF scheme (Shu and Osher, 1989). For the 2nd and 3rd order terms, a modification is made by which a weighted average is used in place of the two candidate divided differences,

$$D_- = D\left[x_{j-1/2}, ..., x_{j+l-1/2}\right], D_+ = D\left[x_{j+1/2}, ..., x_{j+l+1/2}\right], l = 2, 3 \quad (7)$$

hence ensuring the smoothness of the interpolation (as opposed to the original choosing of the quantity with smaller absolute value). That is

$$D = \frac{D_+ W^+ + D_- W_-}{W_+ + W_-}, W_+ = D_-^4, W_- = D_+^4. \quad (8)$$

The above is in fact rather similar to WENO (Jiang and Shu, 1996), but in a much simpler form. In one dimensional ENO-LLF Lax-Friendrich flux splitting, the viscosity coefficient, $\alpha_{j+1/2}$, is chosen by

$$\alpha_{j+1/2} = max||\lambda_j|, |\lambda_{j+1}||. \quad (9)$$

However, for two dimensional schemes, if $\alpha_{i+1/2}$ and $\alpha_{j+1/2}$ are chosen separately in x and y directions', non-physical results may occur when CFL number is larger than 0.5. The difficulty is overcome by defining viscosity coefficient as

$$\alpha_{i+1/2} = \alpha_{j+1/2} = max||\lambda_{i,j}|, |\lambda_{i,j+1}|, |\lambda_{i+1,j}|, |\lambda_{i+1,j+1}||. \quad (10)$$

In our computation CFL is set to 0.9.

Time discretization for fluid dynamic terms is 3rd order TVD Runge-Kutta method (Shu and Osher, 1988). For chemical kinetic integrations, the set of coupled source terms is solved by Selected Asymptotic Integration Method (SAIM), which is a 2nd order accurate algorithm for solving stiff system of ODEs associated with chemical reactions (Young, 1979). Temperature is solved implicitly by iterating between equation of state and thermochemical relation

5

after each Δt_{fluid}. However, for higher accuracy chemical kinetic integrations, temperature is also updated after each Δt_{source}. As the total energy does not change in the midst of concentration changing with chemical reaction, temperature is calculated by the same method (Fedkiw et al, 1997). Fluid dynamic integrations take only a small portion of the computational time while chemical kinetic integrations are very slow comparing with fluid dynamic integrations, and there is no data exchange for chemical reactions between the different grid nodes with time splitting method (see also Oran and Boris, 1987). So it is fairly straightforward to parallelise the chemical kinetic integrations. In the present work, Parallel Virtual Machine (PVM) technique, controlled and synchronized by PVM3.3, is used, in which the computations involved in the solution of the stiff ODEs on all grid nodes are divided into different computational zones and are spread among the different processors (Geist et al, 1994).

3.2   Computational setup and initialization

The numerical simulation models a detonation propagating from left to right in a stoichiometric $H_2 - O_2$ diluted with 70% argon with initial pressure and temperature given as 6.67kPa and 298K, respectively. Firstly, one dimensional detonation is initialized by a strong shock wave, and which comes to a steady detonation velocity of $1625m/s$. Then, the solution is placed on a two dimensional grid serving as the initial conditions for the two dimensional calculation.

In order to keep the detonation front within the computational domain, the grid is set to move at about detonation velocity in the positive x-direction. The right-hand boundary condition is kept in quiescent state. As discussed in Gamezo et al (1999), the left-hand boundary condition is an extrapolated outflow with a relaxation coefficient of 0.05. The boundary conditions imposed on the upper and lower boundaries are symmetry conditions, which correspond to the reflecting channel walls. The moving grid speed is set at a quantity slightly smaller than the steady detonation velocity. A technique is used to keep the detonation front from crossing the boundary by transferring the solution to a spatial location at a short distance on the left when the front is too closed to the right boundary. In this way, the numerical detonation wave is thus observed for very long physical time and ensured free from the effect of initial condition with imposed perturbations. The grid size used for calculating the formation process of regular cellular structure is $0.2mm$, Then the results are projected onto smaller size grids, which are $0.1mm$, $0.05mm$ and $0.025mm$. In all cases, spatial steps are the same in x direction and y direction.

The initial condition is perturbed by introducing random disturbances to the

initial states only for the first time-step of chemical kinetic integrations via

$$e^* = e + \alpha ef. \tag{11}$$

Here e^* is the perturbed total specific energy which encompasses the small fluctuations to the direction of elementary reactions, f is a random value uniformly distributed in $[-1.0, 1.0]$ and α is a fluctuation coefficient of $0 < \alpha < 1.0$, controlling the fluctuation amplitude.

4 Formation of the regular structure

The numerical results show that the formation process of regular cellular structure can be divide into two phases. In the first phase, the triple wave configurations are observed fairly early and as do the irregular cellular detonation front. However, the irregular cellular detonation takes time to adapt itself to the regular and equilibrium mode of detonation front in the second phase.

Figure 1 shows the pressure at different times during the first phase leading to the formation of the triple wave configurations, with $\alpha = 0.3$. The initial disturbances are very small and one can hardly distinguished the difference from the pressure contours (see Fig. 1a). However, as detonation propagates, the disturbances are magnified and many non-uniformed regions are produced (see Fig. 1c). While moving in the transverse direction, the pressure fluctuations in the non-uniformed regions are intensified although the number of those regions decreases gradually. After that, the leading front becomes more and more wrinkled. It is further observed the existence of transverse waves, Mach stems and incident waves which give rise to the triple wave configurations are clearly evident at about $15\mu s$ (see Fig. 1f). These triple wave configurations continue to move irregularly in the transverse direction. After the formation of triple wave configurations in the first phase, more regular cellular structure begins to form in the second phase. In this latter phase, the neighboring configurations move transversely and colliding with each other. Sometimes, after a configuration makes contact with its neighbor, the two triple wave configurations are merged together with the resulting "weaker" configuration being absorbed by "stronger" one (here "stronger" refers qualitatively to higher transverse wave strength). Fairly regular cellular structure can be reached after the detonation has been running for about $200\mu s$. However, our results show the cellular structure is still evolving, and it then gradually changes to a less regular mode. It is only after a very long time of about $1ms$ later, the structure becomes very regular with less transverse wave number.

In the current work, for a 40mm channel height, the transverse wave number formed is found to be 10, while for the 20mm channel, the number is 5. Once

the regular structure is reached, the detonation runs with the same transverse wave equilibrium mode for a further $3ms$, which is the longest time for the current computations. Figure 2 shows the detailed cellular structure in a $20mm$ channel at $2.061ms$; in fact, the same structure occurs at about every $9.23\mu s$, which is called characteristic time of the detonation cell t_{char}. The transverse wave space, that is cell width, computed in this case study is $0.008m$. Even with small fluctuations and calculating through different time interval, the average detonation velocity is found to be $1625m/s$, which is the same as in one dimensional steady results and slightly higher than CJ value (Gordon et al, 1971).

From our numerical experiments, it can be seen that increasing the intensity of initial perturbation by a higher value of α in Eq. 11, the time for the formation of triple wave configuration is shortened slightly. If α is smaller than 0.05, the fluctuations disappears after several μs. However, if α is strong enough for leading to a cellular structure, the same mode regular structure is reached at almost the same time if the channel height is kept the same. This occurs even with $\alpha = 1.0$, which implies that stronger initial perturbation conditions can at best only slightly shorten the first phase but has no effect on the second phase. Usually, different kinds of perturbation methods were used in previous studies. One can surmise that if perturbations of sufficient strength are imposed, all of them can possibly produce cellular structure (Taki et al, 1978; Lefebvre and Oran, 1995; Oran et al, 1998; Gamezo, 1999; Sharpe, 2001). However, the perturbations can and do effect the cellular structure in the first phase. On the other hand, given a sufficient long time elapsed leading to the second phase, the cellular structure in the later phase is independent of the initial perturbations.

5   Structures with different grid sizes

Figures 2 and 3 show the pressure, density, temperature and H_2O concentration with grid size $0.2mm$ and $0.025mm$, respectively. In both figures, the transverse wave is at about the half way of two successive triple point collisions.

For results with $0.2mm$ grid size, the triple wave configuration is shown, but the details around the triple wave point is not clear. The position of a triple wave point itself can also hardly be defined for the poor resolution. There seems a slip line dividing the regions behind the Mach stem and the transverse wave, but not well defined (see Fig. 2b, 2c). Here, a transverse wave can be divided into two parts: one is the part connected to the triple wave point, called the main transverse wave; the other part extends from the the main transverse wave, called extending transverse wave, but there is no distinct

8

turning point between the two parts (see Fig. 2a). The transverse wave also seems extending from the triple wave points smoothly. Therefore, the configuration looks like a single Mach configuration, which is the characteristics of a weak structure. However, the information from chemical reaction leads to a different conclusion. From H_2O concentration contour, the ignition front can be approximated defined by the concentration discontinuity (see Fig. 2d). The ignition front behind the transverse wave show the most notable characteristic of a strong structure. It can be also noted that there is a darker region behind the adjoints of the Mach stem and the transverse wave, which shows lagged ignition and indicates that a weak shock wave exists ahead.

Figures 3 show the detailed regular cellular structure with $0.025mm$ grid size. For the convenience of analyzing, the wave fronts, and the angles of these fronts and triple point track angle are shown in Fig. 4 according to the results in Figs 3. The waves of the structure are labeled as follows: I is the incident wave, its shock pressure is much smaller than $17k$Pa, the shock pressure of leading wave in one dimensional steady detonation at the same gas mixture; M is the Mach stem and its shock pressure is much larger than $17k$Pa; T refers the whole transverse wave; a, b are the first and the second triple points, respectively; S is the first slip line; c is the kink which divide the main transverse wave and the extending transverse wave; straight line ab is a weak shock wave, called the weak transverse wave, whose strength is 0.88; straight line bc is the main transverse wave front, whose strength is 1.70; the extending transverse wave front beyond the kink c is curved; d is the intersection point of a shock wave bd, called the additional shock wave, and the first slip line S. There is an other weak shock wave de, which is the reflection wave of the additional shock wave bd. Between the additional shock wave bd and the main transverse wave bc, there is also a weak slip line S', called the second slip line, which is clearly shown in Fig. 3d of H_2O concentration and Fig. 3c of temperature. Five regions can be classified according to the structure: region 0 is the area ahead the Mach stem and the incident wave; region 1 is the area behind the incident wave and ahead the main transverse wave; the area behind the Mach stem and the weak transverse wave is divided into region 2 and region 3 by the first slip line; the area behind the main transverse wave and the additional shock wave is divided into region 4 and region 5 by the second slip line. The above wave configuration is very alike to that of a double Mach reflection of a shock wave. The main difference between them is that there is no kink c in the later one. For a non-reactive shock wave, a kink always occurs at the reflection wave of transitional Mach configuration. This suggests that the second triple wave configuration in the cellular structure is transitional Mach like, and shows stronger strength than a merely double Mach configuration, and the structure showing a expansion fan like region around the kink (see Fig. 3a).

The ignition fronts RR show stronger ignition behind the Mach stem and the

Table 2
Properties of the structures at different resolutions

Grid size $\Delta x = \Delta y$	Transverse wave parts	Slip line number	Triple wave point number	Additional shock wave	Kink
0.2mm	2	1	1	no	no
0.1mm	3	1	2	no	no
0.05mm	3	1	2	no	no
0.025mm	3	2	2	yes	yes

main transverse wave, and much weaker ignition behind the incidental wave. The induced length (the distance to ignition front to shock wave) behind the incident wave is much longer than that behind the Mach stem and the main transverse wave. It can also be observed the gas mixture after the Mach stem is burned by Mach stem ignition. The gas mixture behind the incident wave is ignited by incident wave, and the main transverse wave. The weak transverse wave, the additional shock wave and it reflection wave on the first slip line are so weak that the ignition of the unreacted region behind them is much lagged. Because the unreacted region is just a narrow triangle region between the two slip lines and the regions beside it have much higher temperature, this region can probably be ignited by the weak transverse wave or heat conduction by mixing of the turbulence boundary layer near the two slip lines. The chemical reaction behind incident wave center is not stable. It is possibly cause by the jet produced at the triple point collision. However, the current numerical results show this instabilities do not effect the features of the structure while the detonation propagates.

The calculated results with different gird sizes show that the structure is strong type, and globe features such as the average detonation velocity and the transverse space are also the same in all cases. However, the flow field is shown by different levels of details with different grid sizes. Some selected features of the structure with different resolutions are given in Table 2. It can be found that the more small grid size is used, the more details of the structure are captured by the calculation. However, these results show a good convergence for the features of the flow as increasing spatial resolutions. However, in coarse solutions, such as for 0.2mm or 0.1mm grid size, many of the structure details lose, especially characteristics of the second triple wave configuration.

Table 3
Change of states in structure before the triple collision

Region	1	2	3	4	5
p/p_o	$18.5 \rightarrow 16.3$	$34.8 \rightarrow 30.3$	$34.8 \rightarrow 30.3$	$49.9 \rightarrow 40.5$	$49.9 \rightarrow 40.5$
ρ/ρ_o	$3.73 \rightarrow 3.56$	$4.28 \rightarrow 4.21$	$5.57 \rightarrow 5.45$	$6.73 \rightarrow 6.31$	$6.91 \rightarrow 6.63$
$T(K)$	$1470 \rightarrow 1256$	$2367 \rightarrow 2160$	$1856 \rightarrow 1661$	$2195 \rightarrow 1928$	$1993 \rightarrow 1837$

6 Evaluation of the Structure

In the structure, the Mach stem and the incident wave change their roles by the collision of the configurations. Therefore, it is convenient to divided the structure evaluation process in three parts: before the triple point collision, through the triple point collision and after the triple point collision.

6.1 Before the triple point collision

Figures 5 and 6 show the density and H_2O concentration at 4 times before triple point collision. The overall feature of the structure is that both the strength of the Mach stem and the incident wave decrease while the two configuration moving close. Tab. 3 gives the change of the states in the structure between at the middle of triple wave collisions and at just before the triple point collision. The main transverse wave decreases its strength from 1.8 to 1.5, but the strength of the weak transverse wave almost does not decreases. By comparing with the wave front angles of the structure at the middle of two collisions, the configuration looks like rotated clockwise about 5° around the first triple wave point, and the angles between the wave fronts have not change much (see Tab. 4). The angle that the configuration gas rotated is just about the deflection of the triple point track angle, which changes from 33° to 39.5^o as the structure moving from the middle of triple point collision to just before the triple point collision. It can be seen that the induced zone extending because of the decay of both the Mach stem and the incident wave. The area

Table 4
Angle changes for wave fronts in the structure before the triple collision

	$Track$	M	I	T_{weaker}	T_{main}
Angle (^{o})	$33 \rightarrow 39.5$	$50 \rightarrow 545$	$85 \rightarrow 90$	$15 \rightarrow 20$	$25 \rightarrow 20$

Table 5
Change of states in structure through the triple point collision

Region	1	2	3	4	5
p/p_o	$16.3 \rightarrow 25.4$	$30.3 \rightarrow 45.6$	$30.3 \rightarrow 45.6$	$40.5 \rightarrow 58.9$	$40.5 \rightarrow 58.9$
ρ/ρ_o	$3.56 \rightarrow 4.0$	$4.21 \rightarrow 4.28$	$5.45 \rightarrow 6.08$	$6.31 \rightarrow 6.45$	$6.63 \rightarrow 6.62$
$T(K)$	$1256 \rightarrow 1903$	$2160 \rightarrow 3107$	$1661 \rightarrow 2370$	$1928 \rightarrow 2648$	$1873 \rightarrow 2512$

Table 6
Angle changes for wave fronts in the structure through the triple point collision

$Track$	M	I	T_{weak}	T_{main}
Angle (^{o}) $\quad 39.5 \rightarrow 10$	$45 \rightarrow 75$	$90 \rightarrow 60$	$20 \rightarrow 0$	$20 \rightarrow 30$

of the unreacted region behind the weak transverse wave is also increasing gradually and make a long dark triangle region (see Fig. 6d). It is also noted that the transverse wave reflects itself earlier before triple point collision (see Fig. 5). The reflected wave then becomes stronger and makes straight line front. The transverse wave collision point moves forward fast (see Fig. 6d).

6.2 Through the triple point collision

Fig. 10 and Fig. 11 show the density and H_2O concentration at 4 times through the triple point collision. The collision process can also be divided into three successive phases: collision of the transverse wave, collision of the the first triple point and collision of the second triple point. Firstly, the transverse wave collides in the induced zone behind the incident wave. This collision is regular reflection and makes new ignition and produces new region with highest pressure. This high pressure and new ignited region spreads quickly along reflection line until the transverse waves colliding totally. In the reflection center, there is very high pressure, about $660kPa$ and propagating in all direction like a explosion wave. Just after the transverse waves collide in the induced zone behind the incident wave, the first triple points collides, which can also be found a regular reflection. That is why the ignition front just after the collision is not vertical to the reflection line but a small angle to the reflection line, showing the ignition front is behind a reflection wave and no Mach stem exis (see Fig. 11b). The second triple point collide lastly, which creates a reflecting wave too for very small wave front angles of the weak transverse wave. Therefore, the three collision processes are all regular reflection. As the

12

collision takes place, the explosion like wave decays quickly and ignites the unreacted region behind the weak transverse wave and make new pressure peak (see Figs. 11c and 11d). As the collision process continuing, the wave configuration changes to new double Mach like configuration (see Figs. 11c and 11d). Between the regular reflections and the double Mach like configuration, it is hard to define an interval weak structure or single Mach configration form the current results. It can also observed that,once the double Mach like configuration formed, a unreacted region behind the weak transverse wave is also produced (see Fig 11c).

Fig. 9 gives the sketched structure according to Fig. 11d and Fig. 10d. Tab. 5 and Tab. 6 show the change of the states and the wave front angles in the structure through the triple point collision. It can be observed that the structure configuration is similar to Fig. 4, but with a explosion like wave front T' behind, which becomes weak at this time and has been changed to a compress wave. The new incident wave I has smaller front angle, and the new Mach stem has larger front angle. Both of them have stronger strength. Besides stronger strength, the transverse wave here is more complicated. The weak transverse wave is almost parallel to the reflecting line, and the main transverse wave is short for the narrow induced zone behind the new incident wave. No kink point dividing the main transverse wave and the extending transverse wave is observed. Actually, the extending transverse wave is under developing and its front is very different from that in Fig. 3a.

6.3   After triple point collision

Fig. 10 and Fig. 11 show the density and H_2O concentration at 4 times after the triple point collision. As the structure moves on, the extending transverse wave front develops to a curved line. The main transverse wave front also becomes longer by igniting more area of induced zone behind incident wave. The kink point between extending transverse wave and the main transverse wave is also produced. Meanwhile the weak transverse wave front becomes longer and the area of the unreacted region also increasing. On the other hand, the compress wave, which is left by explosion like wave through the collision, catches up and is merged with the transverse wave and leave low pressure area at the position of the transverse wave colliding. The ignition of the unreacted region left by the structure before the collision becomes very slow (see Figs. ??b and ??c). As the structure moves to the half way of the next collision, it comes to a mirror reflection of the states show by Figs. 5 and 6. It can be observed that the overall configuration changes little after the triple point collision, but the Mach stem and the incident wave decrease their shock pressure. However, the transverse wave strength does not change much again. It can also be found that the configuration approximately rotates

$20 \sim 25^o$ counterclockwise. Meanwhile, the triple point track angle deflects from 10° to 33°.

7   Transverse track

Smoke foil technique was widely use to study the track of the structure. Usually, high speed flow can remove more soot then lower one, so the tangential velocity discontinue on slip line is recorded to divide the regions behind the Mach stem and the transverse wave in a triple wave configuration. Similarly, in current work, the maximum flow velocities $|\mathbf{v}|_{max}$ on each grid nodes in the time history are recorded to simulating smoke foil track. That is

$$|\mathbf{v}|_{max,i,j} = \left[\left(\sqrt{u^2 + v^2}_{i,j}\right)\right]_{max}, t = 0, t_{end}. \tag{12}$$

Figures 12 and 13 show numerical detonation cells as an analogue of smoke foil tracks and how the tracks are left while the transverse wave front sweeping, respectively. Similar to an experimental detonation cell, a numerical cell here has convex curvature tracks in the first half cell and concave tracks in the second half cell. The track left by the forward jet at the cell apex is shown clearly in a numerical detonation cell and there are also weak small tracks just before the triple point collision showing the left unreacted region of the structure being ignited by the regular reflecting wave of the transverse wave. (see Fig. 12).

Generally, It can observed three tracks for each configuration (see Fig. 13). The first track is made by tangential velocity discontinuity on the first slip line S for the strong velocity discontinue between the regions behind the Mach stem I and the weak transverse wave ab. The second track is made by tangential velocity discontinuity on the second slip line S' , for the velocity discontinue between the regions behind the main transverse wave ab and the additional shock wave bd. There is another track, the third track, is made by region near the kink point c on the transverse wave. By comparing with structure details in Fig. 3d, it can found this region corresponds to intersection area of the ignition fronts behind the main transverse wave and the incident wave. Of the three tracks, the first track is the strongest one for largest velocity discontinuity between the first slip line, and the third track is the weakest for the weak expansion like configuration, which gives almost continuous transition (see Fig. 12). The third track around the triple wave collision shows the lengthening process of the main transverse wave front with the increasing area of the induced zone behind the incident wave.

Table 7
Comparisons numerical results to experimental marginal detonation (VMT, 1963)

Parameters	Numerical results	Experiments
Mach stem front angle (^{o})	50	64
Incident wave front angle (^{o})	85	80
Main transverse wave front angle (^{o})	25	30
Triple point track angle (^{o})	33	30
Weak transverse wave strength	0.88	1.26
Main transverse wave strength	1.7	5.3

8 Comparison with experiments and previous calculations

The strong structure obtained form current simulation are in good agreement with the ones reconstructed form schlieren photographs of marginal planar and rectangular cellular detonation by VMT (Voitsekhovskii, Mitrofanov and Topchian) (1963) and Strelow and Crooker (1974), including the two triple points a and b, the two slip lines S and S', the transverse wave T. The numerical results also gives the location of reaction zones difficult to obtain from experiments. Both numerical and experimental results show the weak transverse wave front is short comparing to that of the main transverse wave. The front angles of the Mach stem, the incident wave, the main transverse wave and the triple point track angle are all close to that of experimental data. Tab. 7 show the comparisons between the numerical results and experimental data from VMT (1963). In the reconstructed structure, the third and the fourth triple points are supposed around the region of the intersection of ignition fronts behind the transverse wave and the incident wave. These triple points are not found in numerical results, instead of an expansion wave like configuration showing much weaker waves around here. The calculated strength of the main transverse wave is also only about one third that of VMT's results. This indicates the calculated structure is much weaker than that of a marginal detonation structure. Lefebvre and Oran (1995) and Oran (1998) did simulation with detailed chemical reaction model by using grid sizes about $0.2mm$, and also suggested strong structure. However, the wave configuration can not be well defined for the poor resolution, especially wave fronts around the second triple point. Sharpe (2001) simulated the structure with simple reaction model. He also obtained strong structure, but shown much longer weak transverse wave. The straight line front of the main transverse wave beyond the second triple point was also lost, but being replaced a smooth curved front. This indicates that the main transverse wave are fairly weak, which also show-

15

ing chemical reaction is unfinished behind it. Actually, this is a characteristic of a weak structure. Another difference is that Sharpe obtained a strong kink at the Mach stem. In current results, it only exists in a weak form at near the first triple point form the concentration plot just after the triple point collision (see Fig. 3d). This strong kink has also not been found in experiment work, but shown in other numerical results with simple chemical reaction models too (Zhang et al, 2001).

According to the qualitative picture shown by Strehlow and Crooker (1974), just after the triple point collision, the structure appears to be weak type, and becomes strong type some time later. The current results indicated the structure just after the collision is regular reflection, this is supported by the typical ignition front behind a reflection wave instead of the Mach stem. However, the results shows the regular reflection configuration changes quickly to a double Mach like configuration. The numerical results also show, after the triple point collision the structure configuration changes gradually, in which a kink point created on the transverse wave show the difference of ignition and non-ignition. The Strehlow and Crooker's picture also shows lengthening process of the main transverse wave, however, the transverse wave is sharply cut by other triple points. Another noted characteristic of the structure is, before and after the triple point collision, the structure configuration looks like rotated around the first triple point in the direction of the triple point track deflection. This result is again in agreement with the results of Urtiew et al (1978). Lefebvre and Oran (1995) suggested structure beginning as weak type and changing to strong type gradually. However, their results is based on coarse grid and it is difficult to make conclusion. Sharpe (2001) showed the triple collision is similar to a double Mach reflection. May be the calculated main transverse wave is too weak to make enough ignition by its collision, and makes the collision process like a reflection of non-reaction shock wave.

Even a strong structure has been obtained in this simulation, the numerical cells are in excellent agreement with detonation cells in ordinary detonations, instead that of marginal one (Fickett and Diavis, 1979). This can be found by comparing the transverse wave strength and the third track strength. Another difference supporting this is that there is no tracks which is left by the third or the fourth triple point in triple wave collision of a marginal detonation structure (Strehlow and Crook, 1974). On the other hand, if the experimental smoke foil tracks of a ordinary detonation cell are carefully checked, the so called "single track" is actually a narrow band (Fickett and Davis 1979). In this band, less soot is removed comparing regions neighboring it. By comparing the band with Figs. 12 and 13, it can found that the two sides of this band are just the first track and the second track. The third track calculated in numerical simulation has not been observed in experiments. However, Strehlow and Crook's (1974) work showed even for marginal detonation the third track does not always leave it track on the smoke foils. Therefore, for much weak

Table 8
Comparisons of results of numerical simulation and experimental ordinary detonation

Parameters	Numerical simulation	Experiments
mean detonation velocity ($\bar{D}/D_{CJ}$)	1	~ 1
Transverse wave strength	1.7/0.88	0.5
Cell width length ratio(d/l)	0.55	$0.5 \sim 0.6$
Transverse wave track angle (^{o})	30	$30 \sim 33$
Transverse wave track lines	2[a]	2

[a] The third track is not included.

third tracks in current results, they are also very possible not been recorded by smoke foils, and only the two stronger, the first and the second tracks are mainly recorded. Table 8 gives comparisons of the parameters of the calculated detonation and the experimental ordinary detonation. It can be found the two are in very good agreement, except the transverse wave strength. However, the transverse wave strength is difficult to measure, especially for ordinary detonation (Fickett and Davis 1979). Therefore, the calculated detonation is more like a ordinary detonation than a marginal one. By recording energy release, Lefebvre and Oran (1995) and Oran (1998) obtained similar numerical cells. But with low resolution, they could not show well defined cell tracks. Sharpe (2001) tried to interpreted the third track by numerical simulations. However, the third track he referred may be the second track. For the transverse wave in his results is so weak and no strong ignition behind it, it was hardly to find the third track at all.

9 Conclusion remarks

In this paper, two dimensional simulation of the structure of cellular detonations have been performed with detailed chemical reaction model. In the simulation, regular structure is firstly produced about $1ms$ after very small perturbations introduced at the first time step. The calculations are done with different grid size. While showing good convergence feature, a very high resolution structure has been produced with grid size $0.025mm$.

The calculated structure shows a double Mach like strong structure, but with a stronger reflection wave at the second triple wave configuration. The triple point collision process has been found compromising three successive regular reflection process, and then quickly changes to a double Mach like config-

uration. These results have not been found in calculation with coarser grid or simple chemical reaction models. By comparisons with experimental data and previous calculations, it is found the calculated structure is weaker than that of a marginal detonation. On the other hand, the experimental ordinary detonation cells are re-checked, found to be double-track cells and in agreement with the simulated cell tracks. This result concludes a strong structure for even ordinary detonations. The strong structure has the same characteristics as to that of marginal detonations but weaker strength. Therefore, the presence of a strong structure may not be used as the criterion for deciding wehether an ordinary or marginal detonation exists. However, as a marginal detonation has stronger main transverse wave, the transverse wave strength may be concerned as an important factor to decide the detonation type.

References

[1] Fedkiw RP, Merriman B, Osher S (1997) High Accuracy Numerical Methods for Thermal Perfect Gas Flows with Chemistry. *J. Comput. Phys* **132** 175-190

[2] Fickett W, Davis WC (1979) *Detonation* (Berkeley: University of California)

[3] Gamezo VN, Desbordes D, Oran ES. (1999) Formation and Evolution of Two-dimensional Cellular Detonations. *Combust. Flame*, **116** 154-165

[4] Geist A, Beguelin A, Dongarra J, Jiang W, Manchek R, Sunderam, V (1994) PVM 3 user's guide and reference manual. *ORNL/TM-12187*

[5] Gordon S, McBride B J (1971) Computer Program for Calculation of Complex Chemical Equilibrium Compositions, Rocket Performance, Incident and Reflected Shocks, and Chamman-Jouget Detonations. *NASA SP273*

[6] Jiang GS, Shu CW (1996) Efficient Implementation of Weighted ENO Schemes. *J. Comput. Phys* **126** 202-228

[7] Lefebvre MH, Oran ES (1995) Analysis of shock structures in regular detonation. *Shock Waves* **4** 277-283

[8] Oran, E S, Broris, J P (1987) *Numerical Simulation of Reactive Flow* (New York:Elsevier)

[9] Oran ES, Weber JE, Stefaniw EI, Lefebvre MH, Anderson JD (1998) A Numerical Study of Two-dimensional H2-O2-Ar Detonation Using A Detailed Chemical Reaction Model. *Combust. Flame* **113** 147-163

[10] Quirk JJ (1993) Godunov-type schemes applied to detonation flows *AD-A265482*

[11] Sharpe GJ (2001) Transverse waves in numerical simulations of cellular detonations *J. Fluid Mech.* **447** 31-51

[12] Shu WC, Osher S (1989) Efficient implementation of essentially non-oscillatory shock-capturing schemes, II.*J. Comput. Phys* **83** 32-78

[13] Strehlow RA, Crooker AJ (1974) The structure of marginal detonations. *Acta Astronautica* **1** 303-315

[14] Stull DR (1971) *JANAF Thermochemical Tables, National Standard Reference Data Series, No. 37. 2nd Ed.* (Gaithersberg: U. S. National, Breau of Standrads)

[15] Young TR (1979) CHEMEQ-Subroutine for solving stiff ordinary differntial equtions *AD-A0835545*

[16] Urtiew PA (1976) Idealized two-dimensional detonation waves in gaseous mixtures *Acta Astronautica* **3** 187-200.

[17] Wilson GJ, MacCormack RW (1990) Modeling supersonic combustion using a fully-implicit numerical method *AIAA-90-2307*

[18] Zhang ZC, Yu ST, Hao H (2001) Direct calculations of two- and three dimensional detonations by an extended CE/SE method *AIAA-2001-0476*
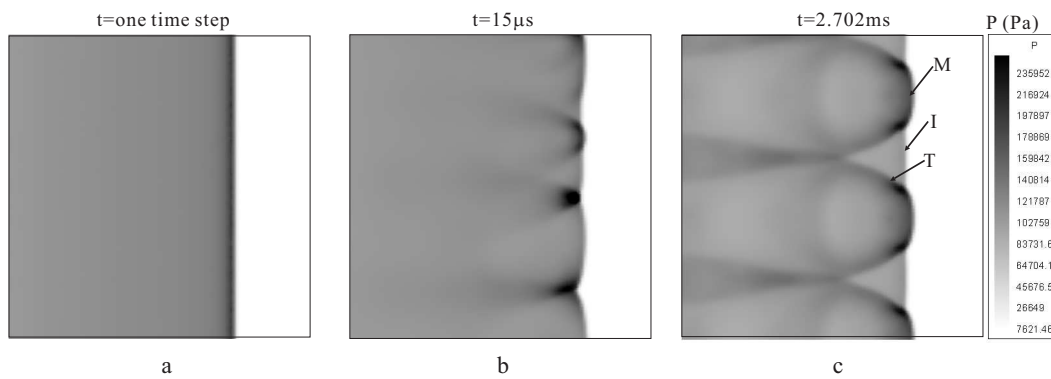
Fig. 1. Pressure contours leading to the formation of triple wave structures, channel height is $40mm$. a)$t = 0$, b)$t = 3\mu s$, c)$t = 6\mu s$, d)$t = 9\mu s$, e)$t = 12\mu s$, f)$t = 15\mu s$, g)$t = 18\mu s$, h)$t = 21\mu s$, i)$t = 24\mu s$, j)$t = 27\mu s$
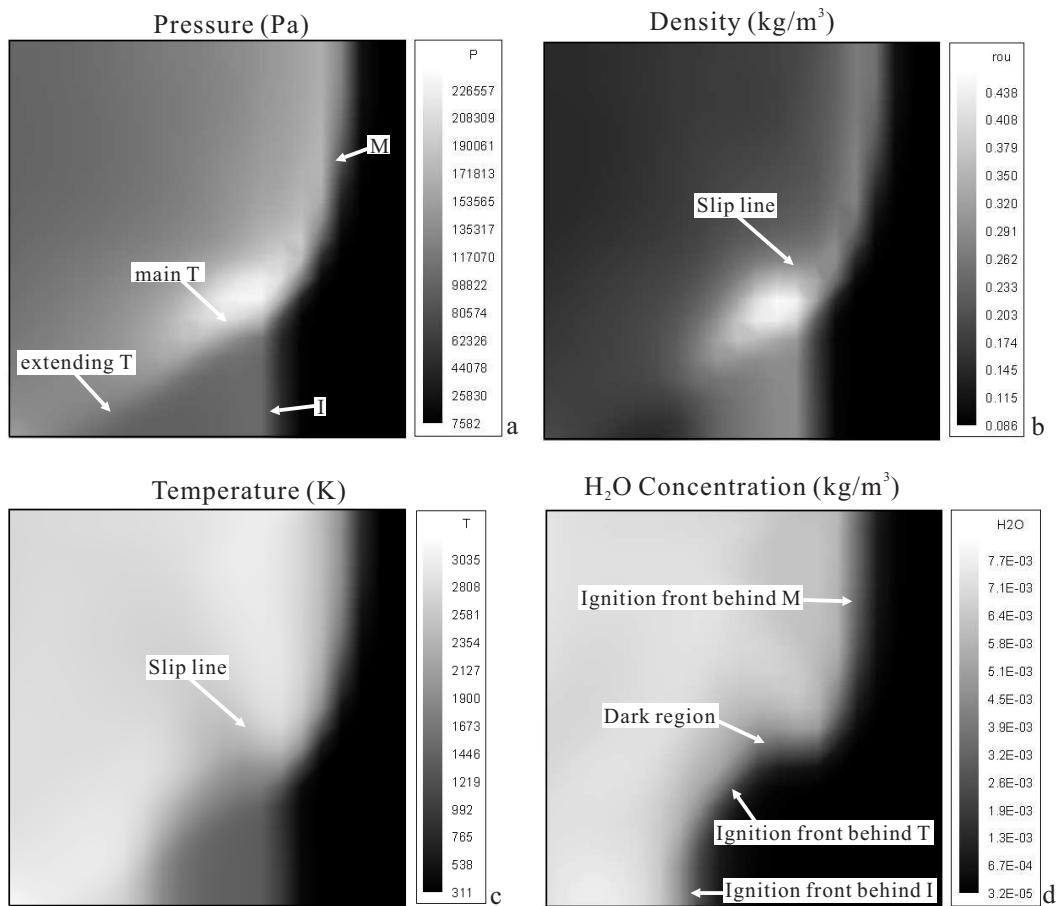
Fig. 2. Regular cellular structure with $0.2mm$ grid size, channel height is 20mm, a)pressure, b)density, c)temperature, d)H_2O concentration
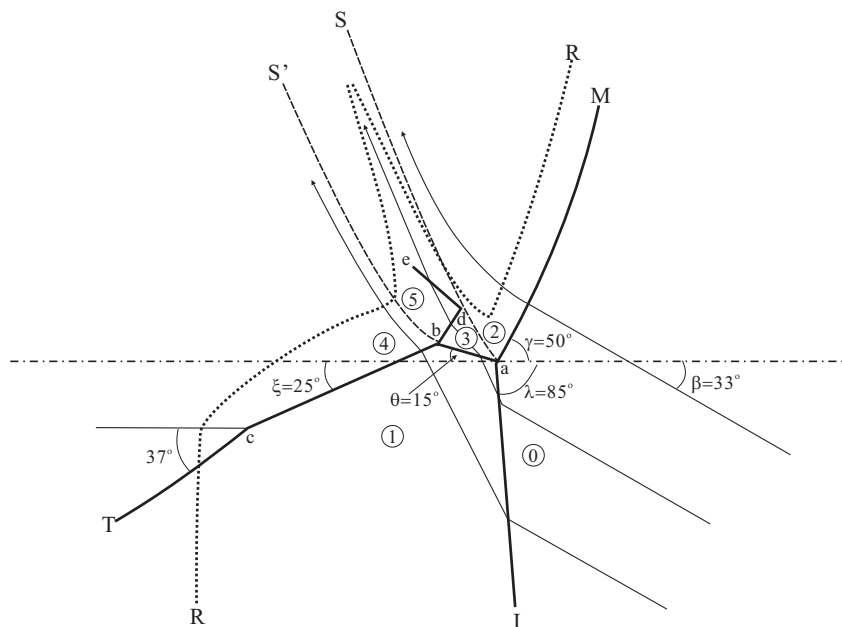
Pressure (Pa)

a

Density (kg/m³)

b

Temperature (K)

c

H₂O Concentration (mol/m³)

d
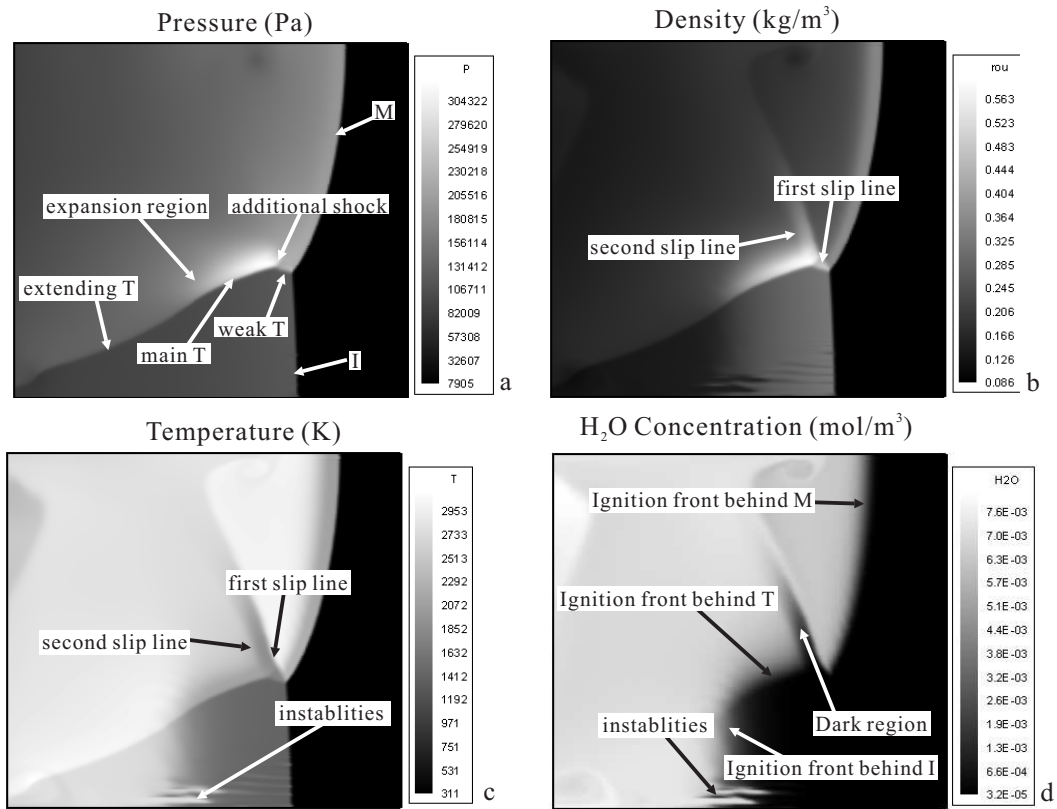
Fig. 3. Regular cellular structure with $0.025mm$ grid size, channel height is 4mm, a)pressure, b)density, c)temperature, d)H_2O concentration

Fig. 4. Detailed structure of a cellular detonation

21
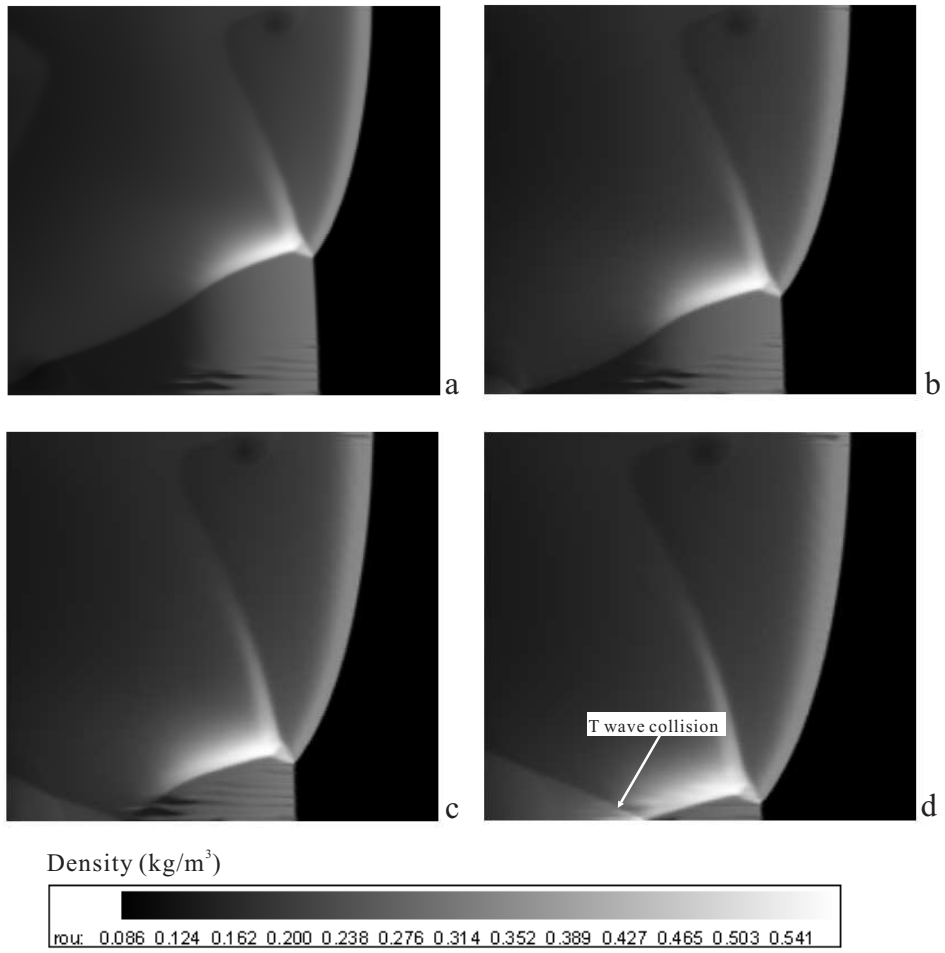
Fig. 5. Density at 4 times before the triple collision, interval between each frame is $0.4\mu s$
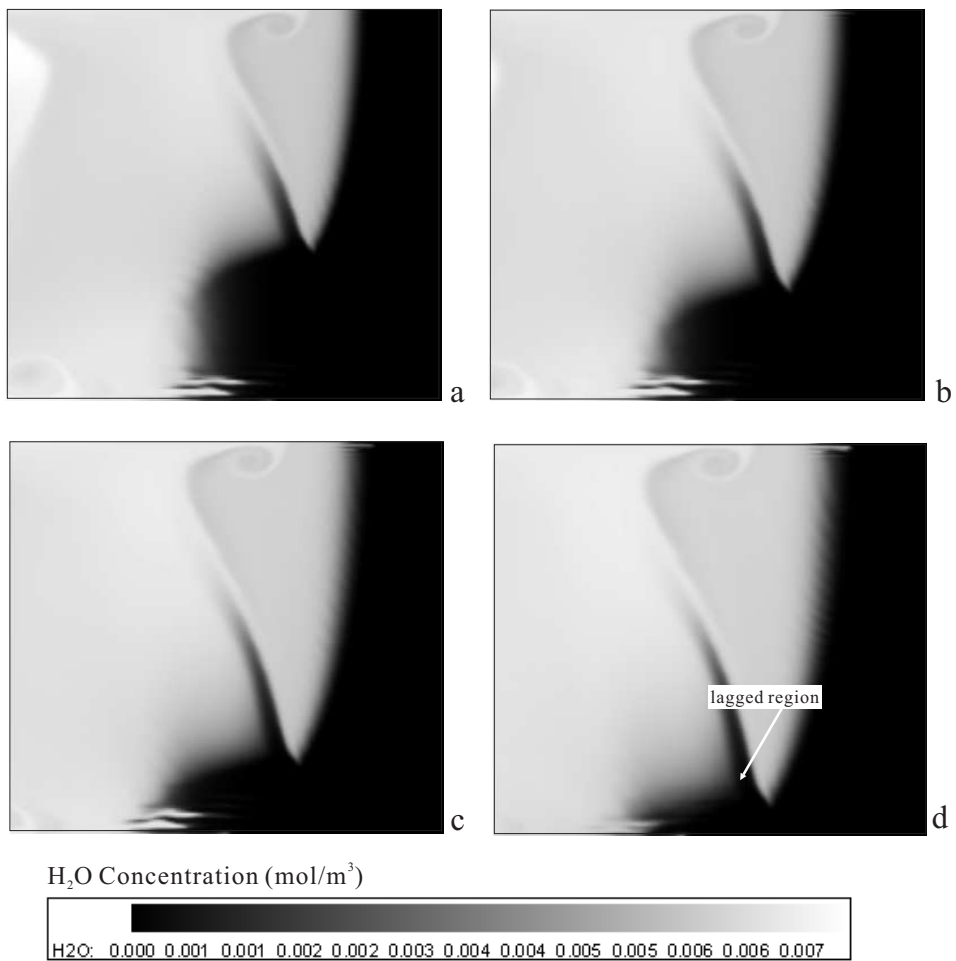
Fig. 6. H_2O concentration at 4 times before the triple collision, interval between each frame is $0.4\mu s$
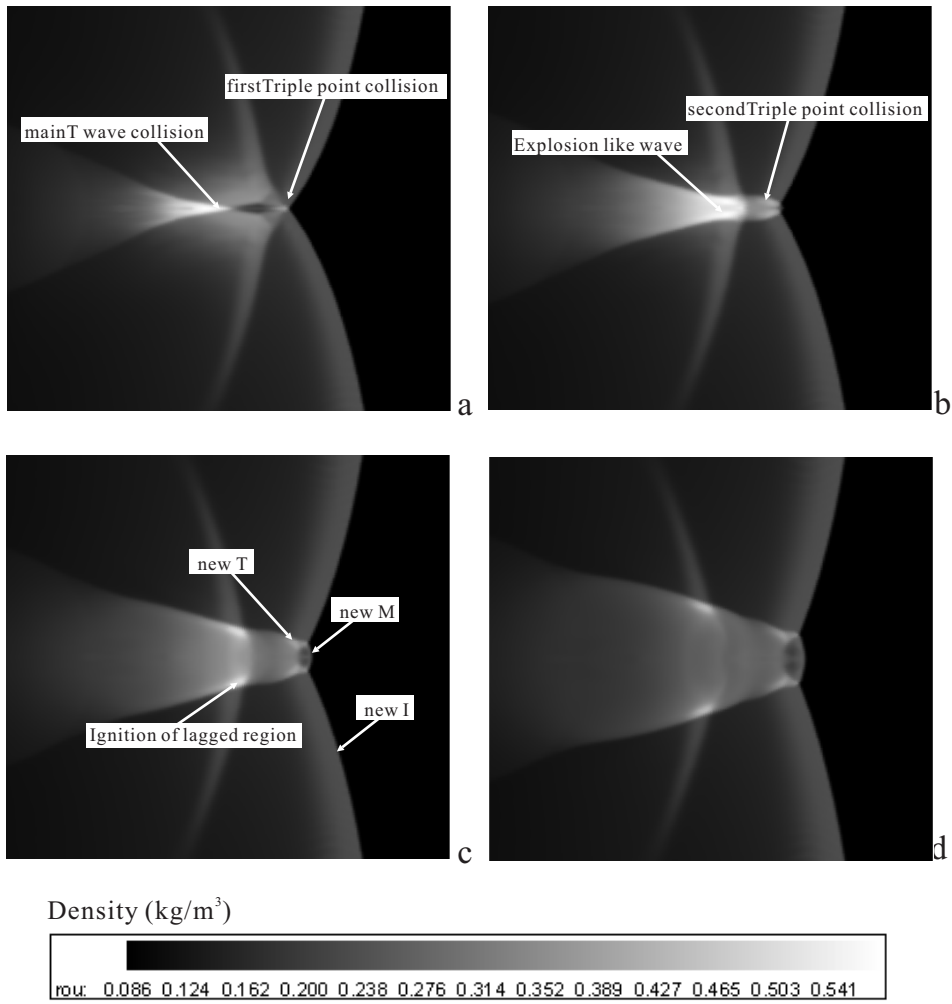
Fig. 7. Density at 4 times through the triple point collision, interval between each frame is $0.1\mu s$
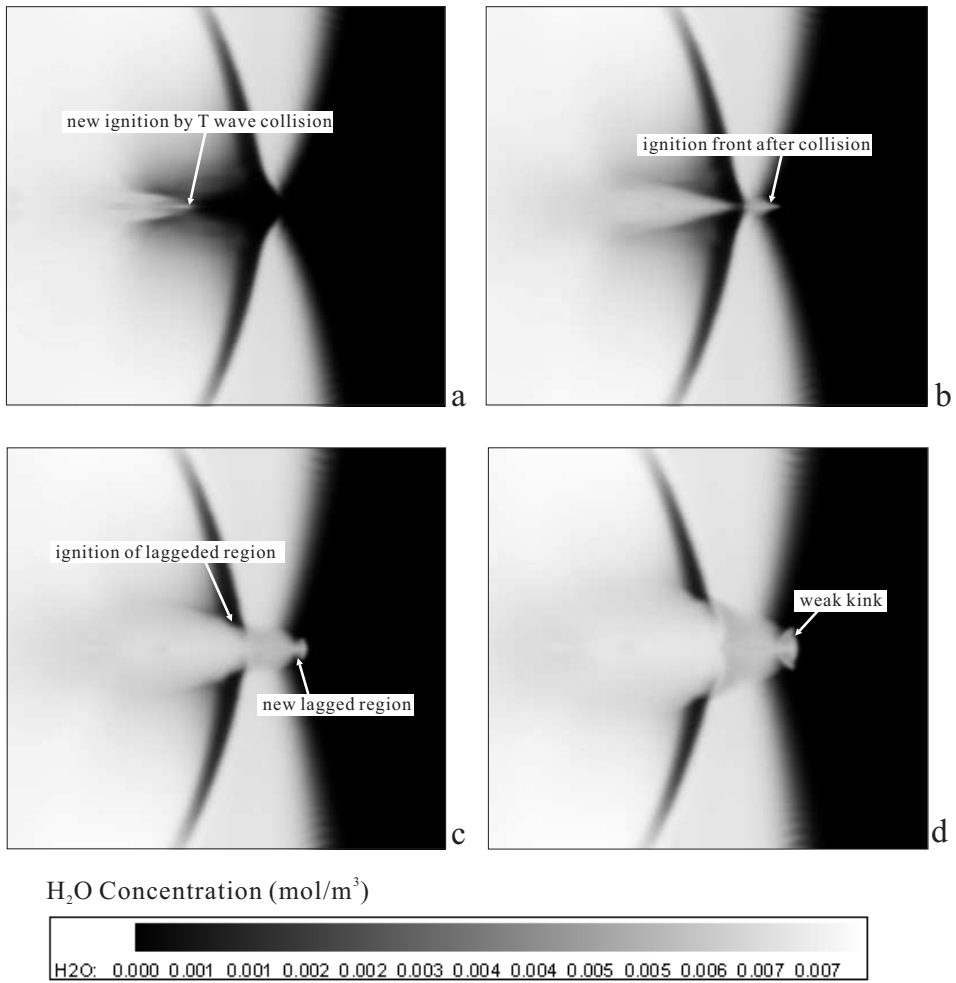
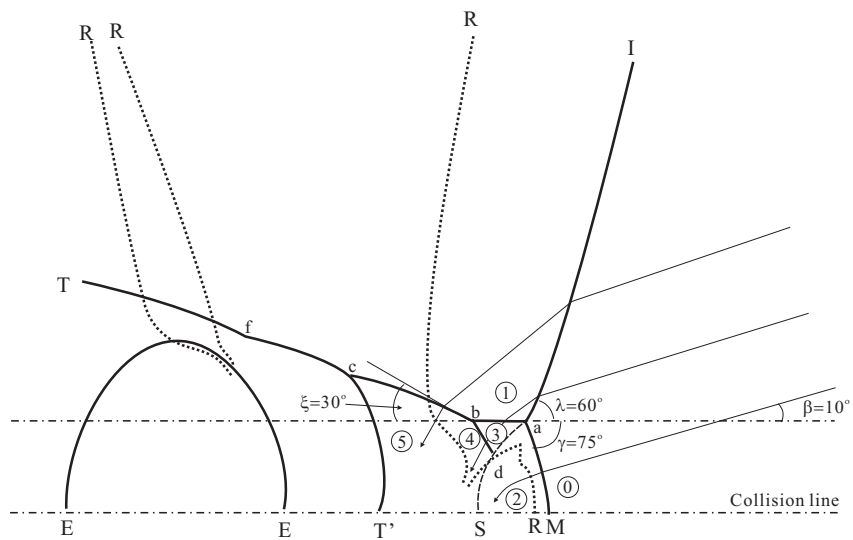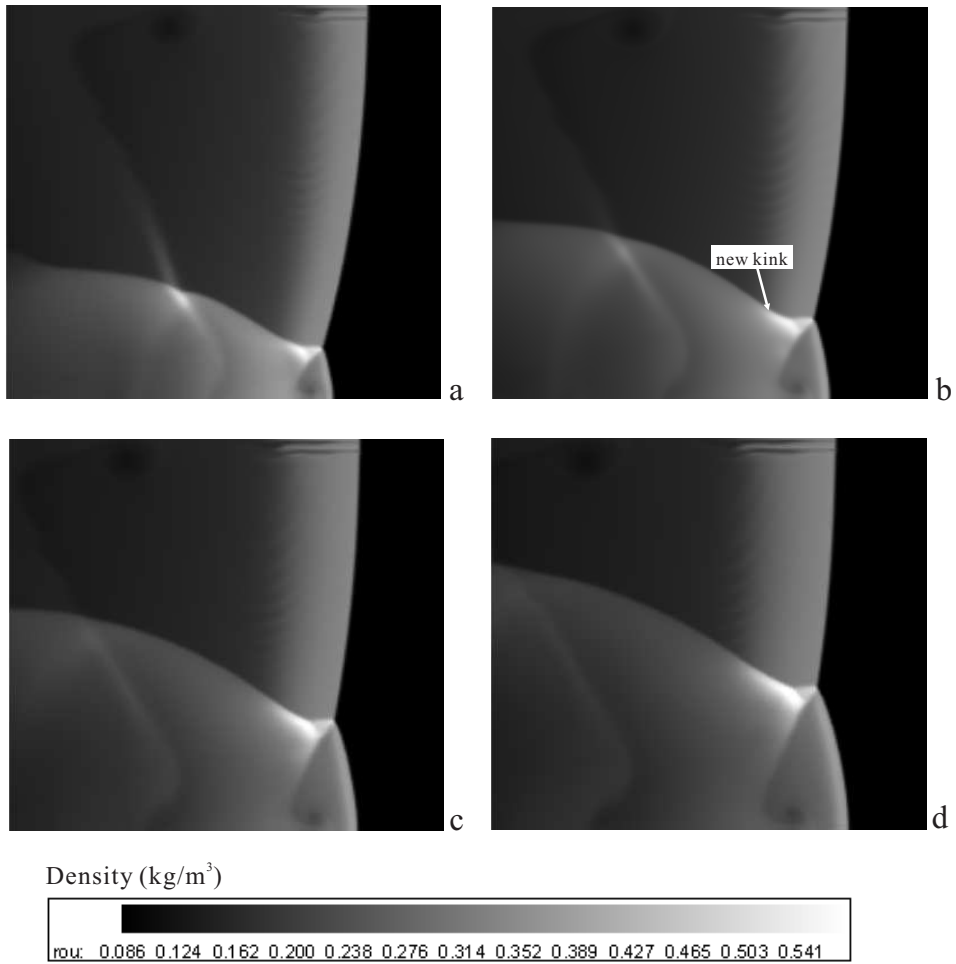Fig. 8. H_2O concentration at 4 times through the triple point collision, interval between each frame is $0.1\mu s$

Fig. 9. Detailed structure of a cellular detonation just after the triple collision

25

new kink

a b c d

Density (kg/m^3)

rou: 0.086 0.124 0.162 0.200 0.238 0.276 0.314 0.352 0.389 0.427 0.465 0.503 0.541

Fig. 10. Density at 4 times after the triple point collision, interval between each frame is $0.4\mu s$
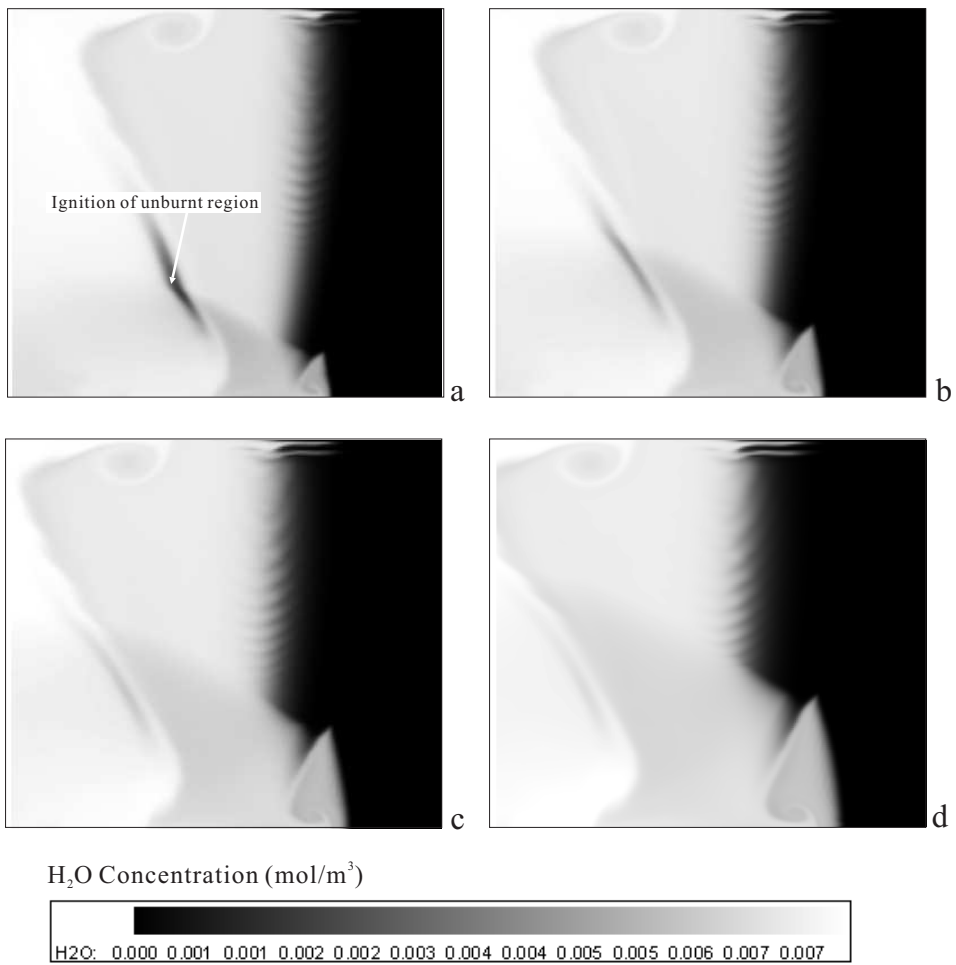
Fig. 11. H_2O concentration at 4 times after the triple point collision, interval between each frame is $0.4\mu s$
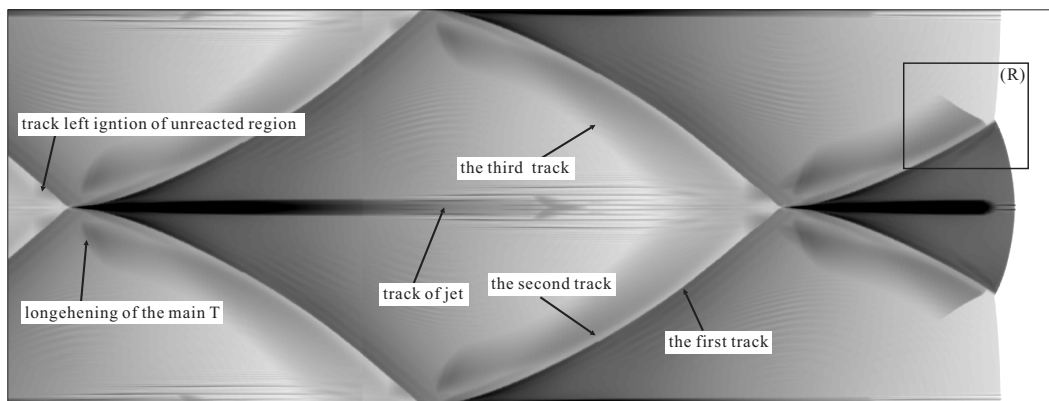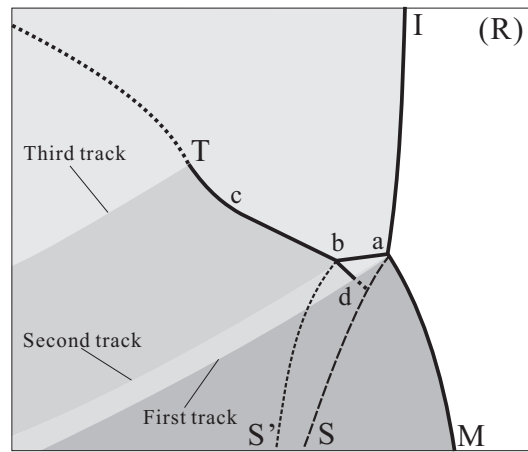

Fig. 12. Numerical detonation cells in a $9mm$ channel

27

Fig. 13. Making structural tracks in a numerical detonation cell